PLOS | BIOLOGY

RESEARCH ARTICLE

Host Gut Motility Promotes Competitive Exclusion within a Model Intestinal Microbiota

Travis J. Wiles[1☯], Matthew Jemielita[2☯¤a], Ryan P. Baker[2], Brandon H. Schlomann[2], Savannah L. Logan[2], Julia Ganz[3¤b], Ellie Melancon[3], Judith S. Eisen[3], Karen Guillemin[1], Raghuveer Parthasarathy[2]*

1 Institute of Molecular Biology, University of Oregon, Eugene, Oregon, United States of America, **2** Department of Physics, University of Oregon, Eugene, Oregon, United States of America, **3** Institute of Neuroscience, University of Oregon, Eugene, Oregon, United States of America

☯ These authors contributed equally to this work.
¤a Current address: Department of Molecular Biology, Princeton University, Princeton, New Jersey, United States of America
¤b Current address: Department of Integrative Biology, Michigan State University, East Lansing, Michigan, United States of America
* raghu@uoregon.edu

OPEN ACCESS

Citation: Wiles TJ, Jemielita M, Baker RP, Schlomann BH, Logan SL, Ganz J, et al. (2016) Host Gut Motility Promotes Competitive Exclusion within a Model Intestinal Microbiota. PLoS Biol 14(7): e1002517. doi:10.1371/journal.pbio.1002517

Academic Editor: Jeff Gore, MIT, UNITED STATES

Received: March 22, 2016

Accepted: June 21, 2016

Published: July 26, 2016

Data Availability Statement: All relevant data are provided within the paper and its Supporting Information files. All data values plotted in figures (main and supplemental) are tabulated in the supplemental spreadsheet "S1 Data." Underlying raw image data (roughly three terabytes in size) are available from the authors by request.

Funding: Authors received funding from the National Science Foundation (NSF, http://www.nsf.gov/), grant no. 1427957 to RP, and the National Institutes of Health (NIH, http://www.nih.gov/), P50GM09891 to KG, P01HD22486 to JSE, and F32AI112094 to TJW. Additional support was provided by the Research Corporation for Scientific

Abstract

The gut microbiota is a complex consortium of microorganisms with the ability to influence important aspects of host health and development. Harnessing this "microbial organ" for biomedical applications requires clarifying the degree to which host and bacterial factors act alone or in combination to govern the stability of specific lineages. To address this issue, we combined bacteriological manipulation and light sheet fluorescence microscopy to monitor the dynamics of a defined two-species microbiota within a vertebrate gut. We observed that the interplay between each population and the gut environment produces distinct spatio-temporal patterns. As a consequence, one species dominates while the other experiences sudden drops in abundance that are well fit by a stochastic mathematical model. Modeling revealed that direct bacterial competition could only partially explain the observed phenomena, suggesting that a host factor is also important in shaping the community. We hypothesized the host determinant to be gut motility, and tested this mechanism by measuring colonization in hosts with enteric nervous system dysfunction due to a mutation in the *ret* locus, which in humans is associated with the intestinal motility disorder known as Hirschsprung disease. In mutant hosts we found reduced gut motility and, confirming our hypothesis, robust coexistence of both bacterial species. This study provides evidence that host-mediated spatial structuring and stochastic perturbation of communities can drive bacterial population dynamics within the gut, and it reveals a new facet of the intestinal host–microbe interface by demonstrating the capacity of the enteric nervous system to influence the microbiota. Ultimately, these findings suggest that therapeutic strategies targeting the intestinal ecosystem should consider the dynamic physical nature of the gut environment.

Advancement (http://rescorp.org/) and the Gordon and Betty Moore Foundation (https://www.moore.org/) to RP. The funders had no role in study design, data collection and analysis, decision to publish, or preparation of the manuscript.

Competing Interests: The authors have declared that no competing interests exist.

Abbreviations: CFU, colony-forming units; DIC, differential interference contrast; dpf, days post-fertilization; EM, embryo medium; ENS, enteric nervous system; GF, germ-free; LSFM, light sheet fluorescence microscopy; MIP, maximum intensity projection; rRNA, ribosomal RNA.

Author Summary

Hundreds of microbial species thrive within the gut of humans and other animals, where they can influence the health of their host in profound ways. The factors that shape the composition of the resident gut microbiota are not well understood, but identifying them represents an important step toward developing treatments for diseases associated with microbial imbalances. Current experimental approaches poorly capture spatial and temporal aspects of microbial interactions within the gut, and yet these features may hold clues to what determines the composition of the microbiota. To address this issue, we used state-of-the-art live imaging to track two bacterial species within the intestine of a model vertebrate host, the zebrafish. We observed strikingly different interplay between the spatial organization of each population and the intestine's peristaltic activity. As a result, one species dominates while the other experiences sudden drops in abundance, the dynamics of which are predicted by a stochastic mathematical model. From this work, we conclude that the composition of indigenous microbial communities may, in part, be shaped by a combination of the physical intestinal environment and the spatial structure of bacterial populations.

Introduction

Trillions of microbial cells representing hundreds of species make up the human intestinal microbiota. This multispecies symbiont supports activities as diverse as host development, nutrient acquisition, immune system education, neural function, and defense against pathogens [1–5]. Changes in microbiota diversity and functional composition have been linked with a variety of human disorders, including obesity, colon cancer, opportunistic infection, and inflammatory bowel disease [6,7]. A major goal of host–microbe systems biology is to clarify the ecological factors that determine microbiota integrity by meshing experimental techniques and quantitative modeling. Insights derived from such efforts will inspire the design of novel therapeutic strategies for microbiota-associated diseases.

An unresolved question is whether the host and microbiota function independently or together to govern the dynamics and stability of individual bacterial lineages. Addressing this question requires identifying the interactions that arise within the spatially complex and heterogeneous environment of the vertebrate gut. However, progress toward this goal has been hindered due to the technical limitations associated with directly observing intestinal communities. Typical interrogation of vertebrate intestinal microbiota involves phylogenetic profiling of fecal material using high-throughput sequencing of 16S ribosomal RNA (rRNA) genes. This technique is blind to the spatial structure of microbial communities, which is known in general to strongly influence interactions [8–10] and has recently been predicted to be important for microbiota stability [11]. Sequencing-based studies also have low sensitivity to temporal structure, owing to both experimental and analytic constraints. Experimentally, metagenomic time-series data remain rare and cannot reach the sampling frequencies necessary to capture interactions occurring at the timescales of microbial division or intestinal flux. Analytically, sequencing data yield only relative, rather than absolute, taxonomic abundances, which severely confounds the inference of interaction networks [12,13]. Furthermore, such methods to date have employed deterministic Lotka-Volterra models [12,14,15] that, even with noise terms representing measurement error, neglect the possibility of fundamentally stochastic or discontinuous interactions among constituents.

Because our knowledge of the factors that shape interactions within host-associated ecosystems is incomplete, contemporary theoretical models have been forced to rely on assumptions that may not realistically mirror microbe–microbe and host–microbe relationships. For example, biochemical and physical inputs from the animal host that likely act on microbial constituents are often ignored [16]. It is important to unravel the extent to which microbiota integrity is simply an intrinsic property of the microbes, which could be recapitulated in vitro with co-culture experiments or in silico with bacterial metabolic network models, or an emergent property of the host-microbe system. Developing accurate accounts of the ecological interactions that manifest within the gut will require model systems that enable manipulation of microbial colonization and measurement methods that can characterize microbial populations in vivo with high spatial and temporal resolution [17].

Toward this end, we employ here larval zebrafish as a model vertebrate host coupled with light sheet fluorescence microscopy (LSFM) [18] as a minimally invasive interrogation method to examine population dynamics within a defined intestinal microbiota. Zebrafish larvae are highly amenable to gnotobiotic techniques and can be reared germ-free (GF) in large numbers [19]. At four days post-fertilization (dpf) larvae possess an open and functional digestive tract that is permissive to microbial colonization, the timing of which is controlled by adding bacteria to the water column. Importantly, larval zebrafish share many physiological traits with humans, including aspects of innate immunity, neurological development, and intestinal function [20]. Therefore, interactions between zebrafish and their microbial symbionts are expected to reflect analogous interactions that occur in other vertebrates. LSFM, combined with the optical transparency of larval zebrafish, enables three-dimensional visualization of the entire intestine with single-bacterium resolution, rapid image acquisition to avoid blurring due to intestinal motility, and extended live imaging with low phototoxicity [21,22]. This experimental setup provides an unprecedented opportunity to investigate ecological interactions within the vertebrate intestine at a range of spatial and temporal scales.

With this model system we found that a competitive interaction between two species native to the zebrafish gut, *Aeromonas veronii* and *Vibrio cholerae*, is characterized by large and sudden drops in the *Aeromonas* population, which appear to be driven by mechanical forces related to the contractile motions of the host intestine. The differential stability of these two species can be explained by their distinct biogeography and community architecture. Tracking *Aeromonas–Vibrio* dynamics motivated a quantitative stochastic model with parameters that could be independently derived from traditional abundance measurements and image-based time-series analysis. Ultimately, this model allowed us to predict the consequences of altering the gut environment through genetic disruption of the enteric nervous system (ENS), achieved via mutation of *ret*, a gene locus associated in humans with the intestinal motility disorder known as Hirschsprung disease (OMIM 164761). ENS disruption stabilized the *Aeromonas* population and neutralized its competitive exclusion by *Vibrio*. This work reveals that interspecies competition and the stability of constituents of the intestinal microbiota can be strongly influenced by the physical activity of the host environment—a mechanism that is likely mirrored in larger and more complex host–microbe systems such as the human gut.

Results

Aeromonas and *Vibrio* Exhibit a Competitive Interaction within the Zebrafish Gut

The intestinal microbiota of larval zebrafish is dominated by bacterial lineages belonging to the *Gammaproteobacteria* [23,24]. In a prior investigation we found that two representative isolates native to the zebrafish intestinal tract, *Aeromonas veronii* strain ZOR0001, hereafter

referred to as *Aeromonas*, and a *Vibrio* strain, ZWU0020, similar in 16S rRNA gene sequence to *Vibrio cholerae* and hereafter referred to as *Vibrio*, exhibit a negative interaction in GF larval zebrafish, with populations of *Aeromonas* that were several orders of magnitude lower in di-associations with *Vibrio* than in mono-associations [25]. Interestingly, only a modest suppression was observed in in vitro competition experiments [25]. To begin to untangle the importance of host and bacterial factors in facilitating the in vivo interaction between *Aeromonas* and *Vibrio*, we used a succession assay in which GF larval zebrafish were first colonized by *Aeromonas* to high abundance, and then challenged by invading populations of *Vibrio* (Fig 1A).

We first enumerated total bacterial abundance by gut dissection and standard plating techniques. In mono-associations beginning at 4 dpf and extending 24, 48, or 72 hr *Aeromonas* populations consistently reach 10^4 colony-forming units (CFU) per host (Fig 1B). By contrast, challenge of established *Aeromonas* populations with *Vibrio* over various 24 or 48 hr temporal windows leads to dramatically lower *Aeromonas* abundance as well as increased host-to-host variation and frequent extinction events (Fig 1B). Under these conditions *Vibrio* exhibits only modest deviations in abundance compared to mono-association (S1A Fig). Of note, *Aeromonas* populations are not destabilized upon self-challenge by newly introduced *Aeromonas*, and *Vibrio* does not induce collapses in established *Vibrio* populations (S1B and S1C Fig). These results demonstrate that subsequent waves of colonizing bacteria alone do not account for the observed competitive interaction and that it is interspecific in nature. Moreover, reversing the order of succession shows that founder populations of *Vibrio* can resist *Aeromonas* invasion, indicating that competition is not merely a consequence of colonization order (S1D and S1E Fig). We also verified that competition between *Aeromonas* and *Vibrio* is dependent on the intestinal environment, as there was not an appreciable difference between their abundances during in vitro mono- and co-culture experiments (S1F Fig).

To determine if the abundance of *Vibrio* correlates with a reduction of *Aeromonas* populations in vivo, we performed a time course experiment in which zebrafish colonized with *Aeromonas* were assayed every 3 hr for 12 hr after inoculation with *Vibrio*. We found that *Vibrio* rapidly infiltrates *Aeromonas*-colonized intestines and steadily increases in number over the 12-hr assay period (Fig 1C). Surprisingly, we did not detect a concomitant decline in *Aeromonas*, implying that *Aeromonas* populations do not respond proportionally to the abundance of *Vibrio* (Fig 1C).

Aeromonas Population Dynamics Are Altered during *Vibrio* Challenge

To further explore the interactions driving *Aeromonas*–*Vibrio* competition, we turned to LSFM. Imaging fluorescently marked variants of each species during mono-association revealed that they have noticeably different intestinal biogeographies and behavior (Fig 2). Populations of *Vibrio* largely comprise planktonic, highly motile cells that appear capable of sampling all available regions within the intestine (S1, S2, and S3 Movies). Quantifying the bacterial density along the anterior-posterior axis (Methods), we find that *Vibrio* is most abundant in the anterior bulb (Fig 2B and 2C), with an overabundance within several micrometers of the epithelial wall that may be the result of hydrodynamic interactions (S2 Fig) [26]. By contrast, *Aeromonas* is most abundant in the midgut and largely takes the form of dense aggregates with a smaller subpopulation of motile individuals (Fig 2D and 2E; S4 and S5 Movies).

To identify the temporal dynamics of the two-member community, we performed in vivo live imaging experiments using LSFM starting approximately 2 hr following the challenge of established *Aeromonas* populations with *Vibrio*. Three-dimensional images spanning the intestine were obtained for each species for durations of roughly 12–15 hr at 20-min intervals,

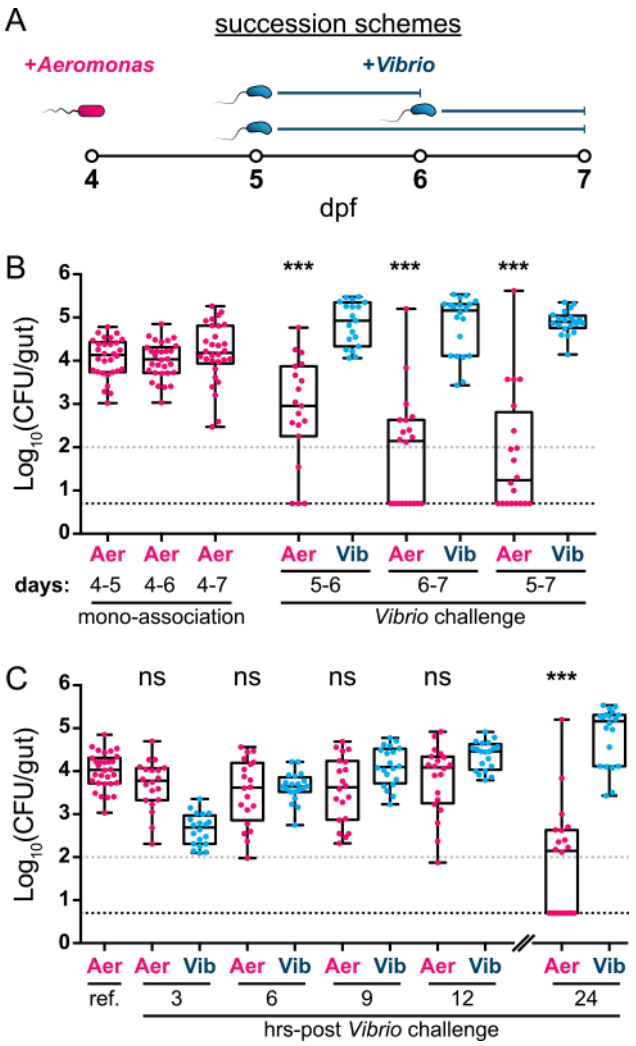

Fig 1. *Aeromonas* and *Vibrio* exhibit a competitive interaction within the larval zebrafish intestine. (A) Graphical overview of succession schemes used to characterize *Aeromonas*–*Vibrio* interactions. *Aeromonas* is allowed to colonize GF larvae at 4 dpf followed by addition of *Vibrio* to the water column at 5 or 6 dpf for 24 or 48 hr prior to enumeration of abundances by dissection and serial plating techniques. (B, left) *Aeromonas* abundances after different mono-association durations and (B, right) *Aeromonas* and *Vibrio* abundances after different *Vibrio* challenge periods. Statistical significance of *Aeromonas* abundances after *Vibrio* challenge compared to respective mono-association reference populations (i.e., 5–6 versus 4–6; 6–7 versus 4–7; 5–7 versus 4–7) was determined by an unpaired *t* test. (C) Time course analysis of *Aeromonas* and *Vibrio* abundances determined by dissection and plating at 3 hr intervals over a 12 hr period starting at 6 dpf. Additionally plotted are an *Aeromonas* mono-association reference population and 24 hr *Aeromonas* and *Vibrio* populations previously plotted in 1B (4–6 and 6–7, respectively). Statistical significance of *Aeromonas* abundances to the mono-association reference population (ref.) was determined by an unpaired *t* test. CFU = colony-forming units; *** = $p < 0.0001$; ns = not significant; $n > 19$/condition. Gray and black dashed lines in panels B and C denote limits of quantification and detection, respectively. Underlying data for B and C are provided in S1 Data.

doi:10.1371/journal.pbio.1002517.g001

which is shorter than each species' approximate 1 hr doubling time (Methods). Fig 3A shows maximum intensity projections of *Aeromonas* and *Vibrio* in a representative larval zebrafish intestine at three time points spanning a 4 hr interval (S6 Movie). The abundance of each species over several hours is plotted in Fig 3B and 3C for 2 fish, representative of 12 fish that we examined. Similar population abundance plots for all zebrafish are provided in S3 Fig. We

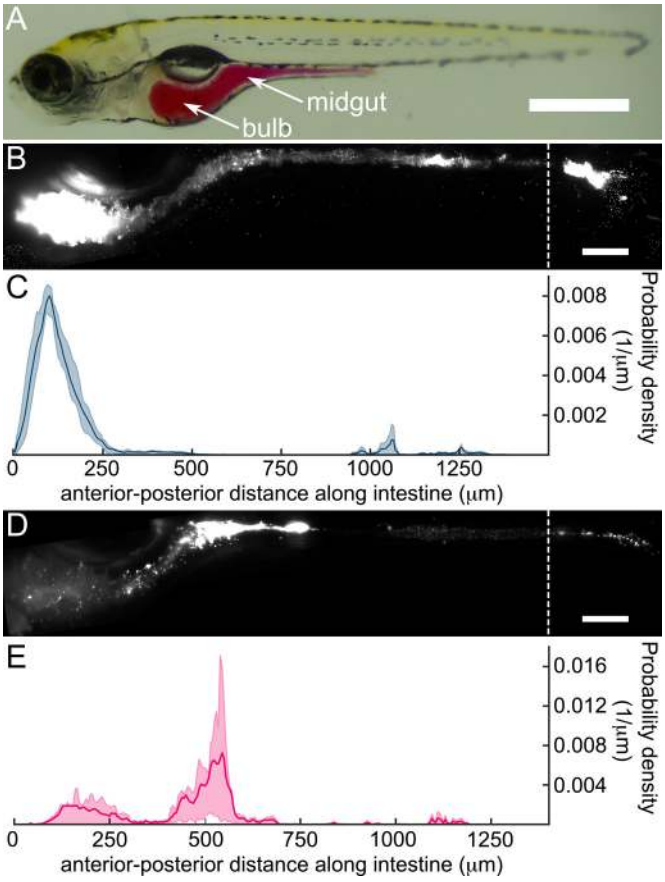

Fig 2. *Vibrio* and *Aeromonas* have distinct community architectures and biogeographies within the larval zebrafish intestine. (A) A larval zebrafish at 5 dpf; the intestine is highlighted by phenol red dye via microgavage [27]. Scale bar: 500 μm. (B) A maximum intensity projection (MIP) of *Vibrio* in the larval intestine. Scale bar: 100 μm. (C) The probability density of *Vibrio* along the intestinal axis. From (B) and (C), we see that *Vibrio* is predominantly localized in the anterior bulb. (D) MIP of *Aeromonas* in the larval intestine. Scale bar: 100 μm. (E) The probability density of *Aeromonas* along the intestinal axis. (D) and (E) show that *Aeromonas* is predominantly localized in the midgut, with a smaller population in the anterior bulb. Underlying data for C and E are provided in S1 Data.

doi:10.1371/journal.pbio.1002517.g002

found that *Vibrio* populations smoothly expand and exhibit a growth rate of 0.8 ± 0.3 hr^{-1} (mean ± standard deviation [SD]), similar to that derived from plating data (0.60 ± 0.22 hr^{-1}, Fig 1C). Strikingly, sharp drops in intestinal abundance, in which the population declines by orders of magnitude within an hour, sporadically interrupt growth of *Aeromonas* (Fig 3A–3C). These local "collapses" appear to be due to *Aeromonas* populations being purged from the gut (S6 Movie). The expelled microbes may still be alive, but are no longer residents of the zebrafish intestine.

To determine if sudden collapses in the intestinal *Aeromonas* abundance occur in the absence of *Vibrio*, we examined live imaging data of *Aeromonas* mono-associations over a similar time frame. We detected clear instances of *Aeromonas* populations sharply declining under these conditions (Fig 3D and 3E). However, in contrast to *Vibrio*-associated collapses, *Aeromonas* was found to consistently recover during mono-association. Additionally, *Aeromonas* collapse events associated with mono-association were smaller and more uniform. Defining collapses as events in which the population decreases by at least a factor of ten within 1 hr, and assigning their magnitude *f* as the ratio of the population after collapse to that before, we find

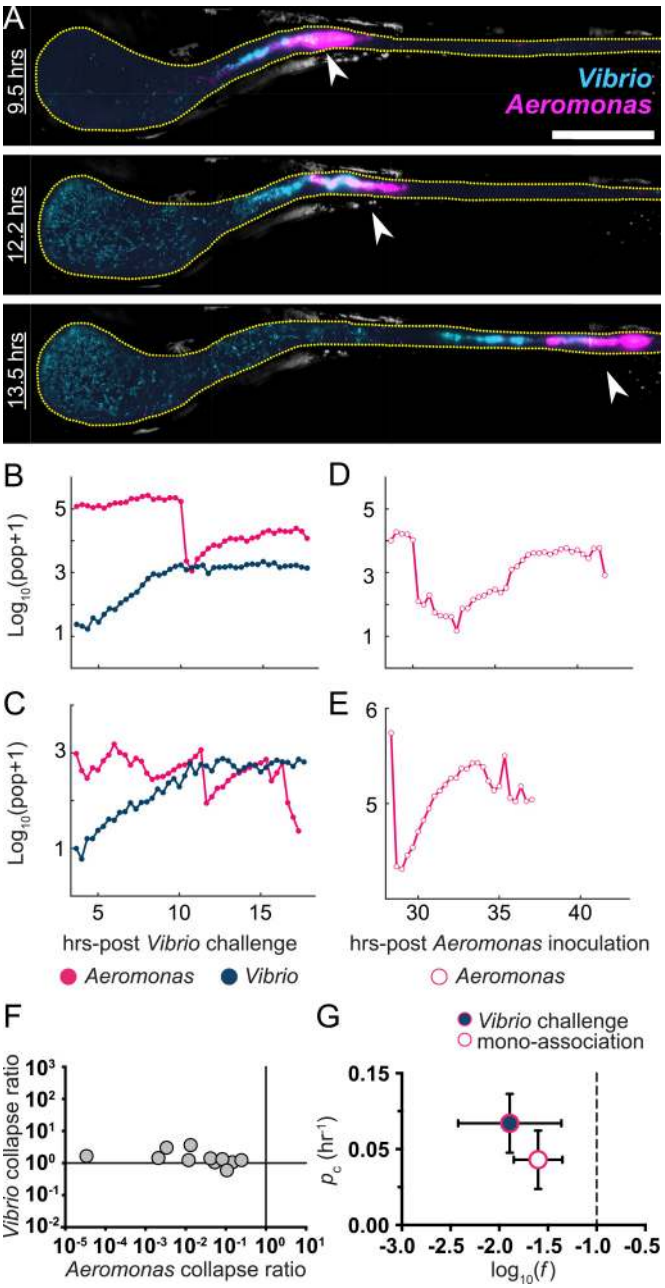

Fig 3. *Aeromonas* experiences sharp drops in population size that are intensified during *Vibrio* challenge. (A) MIPs of *Aeromonas* (magenta) and *Vibrio* (cyan) in a larval zebrafish intestine. Scale bar: 200 μm. The fish was initially colonized at 4 dpf with *Aeromonas*, challenged 24 hr later by inoculation with *Vibrio*, and then imaged every 20 min for 14 hr. The times indicated denote hours post-challenge. In all images, the region shown spans about 80% of the intestine, with the anterior on the left. Image contrast in both color channels is enhanced for clarity. Yellow dotted line roughly indicates the lumenal boundary. As time progresses, the anterior growth of *Vibrio* as well as abrupt changes in the *Aeromonas* distribution (arrows) are evident. (B,C) Total bacterial abundance, derived from image data, for *Aeromonas* and *Vibrio* in two representative fish inoculated and challenged as in panel A, as a function of time following the *Vibrio* inoculation. Sharp drops of over an order of magnitude in the *Aeromonas* population, but not the *Vibrio* population, are evident. (D,E) Total abundance for *Aeromonas* in mono-associations as a function of time post-inoculation, in two representative fish. Sudden declines are also observed, though in general the populations recover to approximately pre-collapse levels. (F) The ratio, *f*, of the abundance immediately after to that before population drops, for *Aeromonas* challenged by *Vibrio*; this ratio spans many orders of magnitude (horizontal axis). At the same time points, the *Vibrio* populations are essentially unchanged, with

ratios of populations afterward to before being close to one (vertical axis). (G) Characteristics of *Aeromonas* population collapses. Circles and bars indicate the mean and standard deviation, respectively, of f and p_c, the magnitude and rate of collapse occurrence, for both mono-associations and *Aeromonas* challenged by *Vibrio*. The dashed line at $f = 0.1$ indicates the threshold for identification of collapses. Underlying data for B–G are provided in S1 Data.

doi:10.1371/journal.pbio.1002517.g003

that for *Aeromonas* challenged by *Vibrio*, $\log_{10}(f) = -1.9 \pm 1.0$ (mean ± SD) (Fig 3F and 3G). The ratio of the *Vibrio* population before and after *Aeromonas* collapse events within the same fish is approximately 1 (Fig 3F), corroborating observations from imaging and plating data that *Vibrio* is resistant to the perturbations that affect *Aeromonas*. We found that during *Aeromonas* mono-associations the magnitude of collapse events was about half of that observed in the presence of *Vibrio*, $\log_{10}(f) = -1.6 \pm 0.4$ (Fig 3G). We also detected a greater rate of *Aeromonas* collapses during *Vibrio* challenge. Estimating the collapse probability per unit time, p_c, as the total number of collapses in all fish divided by the total observation time, we find $p_c = 0.07 \pm 0.02\ \text{hr}^{-1}$ during *Vibrio* challenge and $p_c = 0.04 \pm 0.02\ \text{hr}^{-1}$ during *Aeromonas* mono-associations (Fig 3G), where the uncertainties are estimated by assuming an underlying Poisson process.

Aeromonas and *Vibrio* Are Differentially Resistant to Intestinal Motility

We next inspected the spatial structure and dynamics of each species to uncover clues regarding possible factors driving *Aeromonas*' sudden population drops. A conspicuous feature of the larval zebrafish intestine, like most animal intestines, is that it exhibits periodic motility, with waves of peristaltic contractions that propagate along its length. We found that *Vibrio* populations, being made up of motile, planktonic individuals, are almost completely unaffected by the mechanics of intestinal motility (Fig 4A). Like a liquid filling its container, populations of *Vibrio* quickly adapt to the contracting and expanding space with surprisingly little change in their distribution (Fig 4B; S3 Movie). By contrast, the rigid and largely non-motile aggregates of *Aeromonas*, localized to the narrow midgut, are strongly affected by intestinal contractions (Fig 4C and 4D; S7 Movie). These observations support the hypothesis that forces exerted on this two-member community by intestinal motility give rise to rare and stochastic purging of *Aeromonas* while leaving *Vibrio* largely unperturbed. Corroborating this, we indeed observe posterior transport of *Aeromonas* in collapse events during live imaging experiments (Fig 3A; S6 Movie).

Sudden drops in *Aeromonas* populations occur with or without the presence of *Vibrio*, but these collapses have different significance in the two cases for the overall abundance of *Aeromonas*. One can imagine several possible explanations for this. We first asked whether the intrinsic growth rate of *Aeromonas* post-collapse is lower if *Vibrio* is present. The data show that this is not the case. Mono-associated *Aeromonas* have a growth rate shortly after collapse of $0.74 \pm 0.1\ \text{hr}^{-1}$ (mean ± SD, $n = 5$ collapses), whereas *Vibrio*-challenged *Aeromonas* have $0.64 \pm 0.2\ \text{hr}^{-1}$ ($n = 4$ collapses). We next asked whether the presence of *Vibrio* leads to changes in intestinal mechanics. To test this, we imaged intestinal motility in larval zebrafish using differential interference contrast (DIC) microscopy [28] and calculated the dominant period and amplitude of intestinal contractions. Comparing GF fish with *Vibrio* or *Aeromonas* mono-associated fish, or fish in which *Aeromonas* is challenged after 24 hr by *Vibrio*, there is no notable difference in period or amplitude (S4 Fig). The consequences of intestinal motility on *Aeromonas* collapse properties are clearly different in the mono-association and challenge cases, however, as indicated by changes in collapse magnitudes and rates (f and p_c, Fig 3G). We also note that during challenge experiments, the gross spatial distribution *of Vibrio* is similar to its

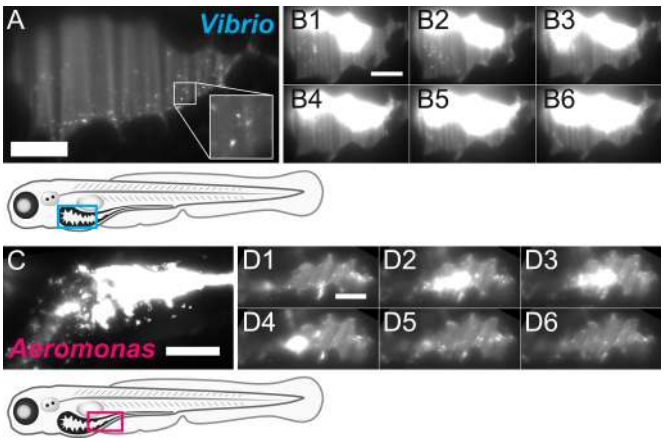

Fig 4. Populations of *Vibrio* and *Aeromonas* exhibit different dynamics within the zebrafish intestine. (A) An optical section of the intestinal bulb from a larval zebrafish mono-associated with *Vibrio* (the cyan box in the diagram below outlines the region imaged). The population consists of discrete, highly motile individuals (inset: single *Vibrio* cells). (B) A montage of images taken from the time-series in S3 Movie shows that the highly motile and planktonic *Vibrio* cells maintain their overall distribution despite repeated intestinal contractions. Time between frames: 1 second. (C) An optical section of the intestinal midgut from a larval zebrafish mono-associated with *Aeromonas* (the magenta box in the diagram below outlines the region imaged). Cells are largely non-motile and densely aggregated. (D) A montage of images taken from the time-series in S7 Movie shows an aggregate of *Aeromonas* in the midgut that is spatially dynamic, entering and exiting the field of view multiple times. Time between frames: 1 second. (A–D) Scale bars: 50 μm.

doi:10.1371/journal.pbio.1002517.g004

distribution during mono-association, whereas there is considerable broadening in the spatial distribution of *Aeromonas* when challenged (S5 Fig). Finally, a conceptually minimal model of interaction is that with *Vibrio* present, the resources available to *Aeromonas* post-collapse are less than with *Vibrio* absent, thereby placing a limit on its potential for recovery. We assess this possibility quantitatively below by estimating carrying capacities, and also examine the consequence of combined changes to the carrying capacity and collapse properties.

The Combination of Stochastic Collapse Events and Competition with *Vibrio* Accounts for *Aeromonas* Population Dynamics

Thus far our data suggest that *Aeromonas* is susceptible to stochastic disturbances mediated by host intestinal motility, and that its recovery from these disturbances is altered in the presence of *Vibrio*. If this is the case, we should be able to build a quantitative model that reflects these data, explains the high variance observed in plating assays (Fig 1), and offers insights into the differential outcomes between mono-association and challenge experiments. The model we construct is illustrated schematically in Fig 5. Consider a bacterial species exhibiting logistic growth, with intrinsic growth rate r and carrying capacity K (Fig 5A and 5B); in other words, the population N grows with time t according to:

$$\frac{dN(t)}{dt} = rN(t)\left(1 - \frac{N(t)}{K}\right).$$

Superimposed on this logistic growth are rare collapses, during which the population drops to f times its pre-collapse value, where f is between 0 and 1, and after which it resumes logistic growth (Fig 5C). The collapses are stochastic and modeled as Poisson processes; i.e., they occur at random with some probability per unit time p_c (Fig 5D). This model arises in many ecological contexts, and some of its mathematical properties have been explored in various studies [29]. Of course, this model incorporates stochastic population drops by construction, and so

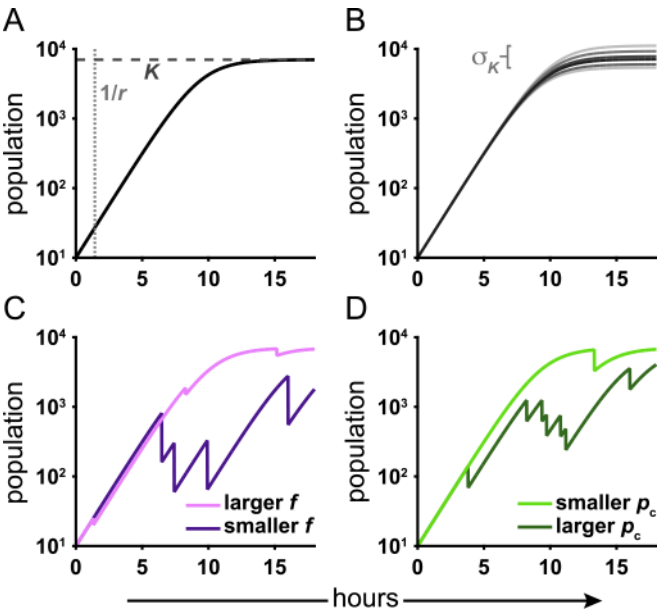

Fig 5. Schematic of a model of growth punctuated by collapses. (A) The model is based on simple logistic growth, which is characterized by two parameters, the growth rate, *r*, and carrying capacity, *K*. (B) We also include a parameter characterizing variability in the carrying capacity. Stochastic collapses are governed by two parameters: (C) the fraction of the population remaining after a collapse, *f*, and (D) the probability per unit time of a collapse, p_c.

doi:10.1371/journal.pbio.1002517.g005

does not predict them from first principles. However, the parameter values that emerge from fitting such a model to the data can, as shown below, yield quantitative insights into the mechanisms underlying the observed dynamics that are not evident from mere visual inspection of the raw data.

Simulating ensembles of populations that exhibit the above dynamics, we examine the mean and, importantly, the standard deviation of the population at discrete terminal time points, as these are statistics that allow direct comparison to results from plating assays. As shown in detail in S1 Text, the apparent dependence of the model on the parameters, *r*, *K*, p_c, and *f*, reduces to two effective parameters. The growth rate, *r*, is both independently known and irrelevant for the conditions considered, and the dynamics depend on the combination $z = -p_c \log_{10}(f)$ rather than on p_c and *f* independently. Values of the two remaining relevant parameters, *K* and *z*, which characterize the carrying capacity and the collapse dynamics, respectively, determine the model predictions for the mean and variance of populations. A grid search through the (*K*, *z*) space for the values that minimize the distance between the predicted and observed *Aeromonas* population statistics gives the best-fit model parameters. Additional details and discussion are provided in S1 Text. It is important to note that because our imaging data revealed that *Aeromonas* is often in a state of experiencing or recovering from purge events, the observed population is likely never close to *K*, and thus we cannot simply use the mean of the bacterial abundance to estimate *K*. Rather, we must use a model to infer the carrying capacity that would yield the observed populations.

Using *Aeromonas* abundance data obtained by gut dissection and plating 24 hr post *Vibrio* challenge (Figs 1B, 6-7), we find best-fit parameters $\log_{10}(K) = 3.2 \pm 0.5$ and $z = 0.13 \pm 0.05$ hr $^{-1}$, the latter providing a constraint on p_c and *f* together. We can *independently* estimate p_c and *f* from imaging-derived data (Fig 3). As noted previously, for *Aeromonas* challenged by *Vibrio*, we find $p_c = 0.07 \pm 0.02$ hr $^{-1}$ and $\log_{10}(f) = -1.9 \pm 0.3$ (mean ± standard error), yielding

$z = 0.13 \pm 0.05$ hr $^{-1}$, which is consistent with the plating-derived value. The agreement between the separately determined measures of z is remarkable, as it indicates that the statistical properties inferred from an ensemble of populations at a discrete time point are consistent with the properties inferred from the temporal dynamics within individual hosts. As expected, $\log_{10}(K)$ is greater than the observed mean *Aeromonas* abundance at 24 hr, since the model-derived K represents an upper bound for the population in the absence of any stochastic collapses or *Vibrio* competition. As another test of consistency, we note that simulating our stochastic model for 48 hr post-challenge using the best-fit parameters determined from plating experiments 24 hr post-challenge predicts a mean and standard deviation of $\log_{10}$(population+1) of 1.3 ± 0.3 and 1.5 ± 0.2, respectively, in agreement with the observed plating values of 1.7 ± 0.3 and 1.6 ± 0.3 (Fig 1B). All of these assessments support the conclusion that the observed population dynamics are governed by a mechanism of stochastic collapse.

We can also apply this model to *Aeromonas* mono-association data. Here, the variance of the plating-derived populations is small (Fig 1B), likely due to comparatively rare and/or weak collapses, as discussed earlier. For reasons described in detail in the S1 Text, this hinders robust determination of z, though K remains well fit. We find that $z = 0.01 \pm 0.01$ hr $^{-1}$ and $\log_{10}(K) = 4.2 \pm 0.1$. From live imaging data, $p_c = 0.04 \pm 0.02$ hr $^{-1}$ and $\log_{10}(f) = -1.6 \pm 0.2$, from which $z = 0.07 \pm 0.03$ hr $^{-1}$ (S1 Text). Our identification of thresholds is, by construction, only sensitive to collapses of a factor of ten or more in magnitude (i.e., $\log_{10}(f) \leq -1$), so our estimate of f, and therefore z, is biased toward larger values.

The above analysis yields insights into the nature of the competition between *Aeromonas* and *Vibrio* that are not obvious from simple visual inspection of the data. The carrying capacity (K) experienced by *Aeromonas*, as estimated by our model, is only one order of magnitude lower in the presence of *Vibrio* ($\log_{10}(K) = 3.2 \pm 0.5$) than when *Vibrio* is absent ($\log_{10}(K) = 4.2 \pm 0.1$). However, the observed abundance of *Aeromonas* is suppressed by more than two orders of magnitude: mean($\log_{10}$(population+1)) = 1.7 ± 0.3 and 4.1 ± 0.1 when challenged by *Vibrio* and mono-associated, respectively (Fig 1B). These results suggest that the combined effect of stochastic collapses, which are likely driven by the intestinal environment, and a reduced carrying capacity, which is a likely result of direct competition for resources with *Vibrio*, has a much greater influence on population dynamics than either mechanism would provide alone.

During *Vibrio* Challenge, *Aeromonas* Populations Are Stabilized in Mutant Hosts Lacking Enteric Nervous System Function

Our data thus far indicate that host-mediated stochastic disturbances are central to the competitive exclusion of *Aeromonas* by *Vibrio* within the larval zebrafish intestine. Therefore, we predicted that if intestinal motility were reduced, *Aeromonas* populations would be stabilized in the face of *Vibrio* challenge. To test this hypothesis, we carried out succession assays in mutant zebrafish hosts essentially lacking a functional ENS due to disruption of the gene encoding the Ret tyrosine kinase, which is critical for ENS development [30]. For these studies, we utilized the *ret1*^{hu2846} mutant allele, which is recessive. Using DIC microscopy to assess intestinal motility, we found that *ret* mutant larvae (*ret* $^{-/-}$) exhibit rhythmic contractions, but with different characteristics than wild-type (*ret*$^{+/+}$) and heterozygous siblings (*ret*$^{+/-}$) (S8 and S9 Movies). Consistent with the recessive nature of this allele, we observed that *ret*$^{+/+}$ and *ret*$^{+/-}$ animals are phenotypically similar with regard to intestinal motility; thus, we refer to both *ret*$^{+/+}$ and *ret*$^{+/-}$ individuals as wild type. Computational analysis of time-series DIC images allows quantification of the displacement of intestinal tissue during contractile waves (Methods). We found that in general the median peak amplitude of longitudinal contractions is greater in wild-type than

in *ret* mutant larvae (Fig 6A). At 5 and 6 dpf specifically, the days on which *Vibrio* is introduced during succession assays, a considerable fraction of *ret* mutant larvae show low amplitudes of motility, whereas wild-type animals exhibit a broader range of amplitudes (Fig 6A).

Though the amplitude of intestinal contractions might not be directly related to the magnitude or rate of *Aeromonas* collapse events, it is reasonable to expect some monotonic relationship between the two, as they both reflect physical activity of the intestine. Therefore, we would expect to observe some degree of stabilization of *Vibrio*-challenged *Aeromonas* populations in *ret* mutant hosts. Indeed, *Aeromonas* populations were able to persist despite *Vibrio* challenge in *ret* mutant hosts from 6 to 7 dpf, and in fact were statistically indistinguishable from a reference *Aeromonas* mono-association (Fig 6B, right). *Vibrio* challenge of established *Aeromonas* populations between 5 and 6 dpf yielded the same decrease in *Aeromonas* abundance in both *ret* mutant hosts and wild types (Fig 6B, left). The difference in competition within *ret* hosts between these two challenge periods may be due to the small increase in the fraction of mutants exhibiting low amplitudes at 6 dpf compared to 5 dpf (Fig 6A). However, in the absence of a

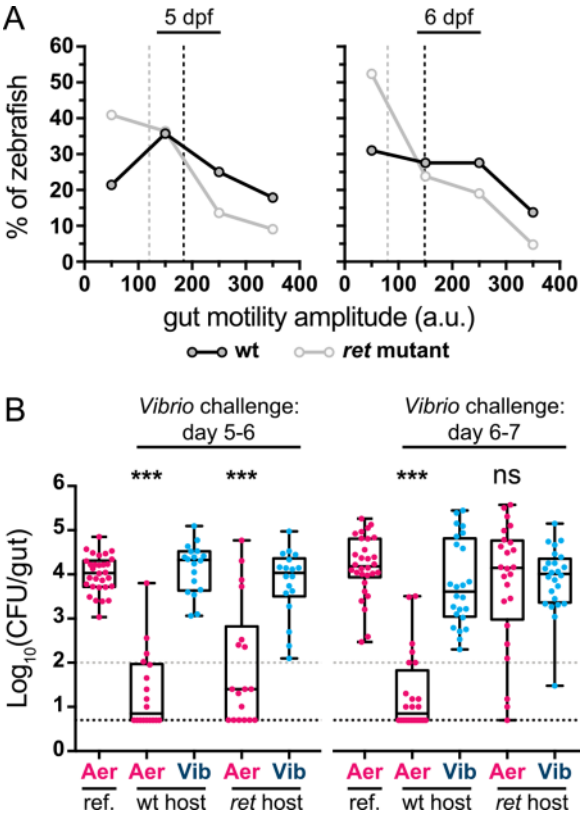

Fig 6. Intestinal motility and bacterial competition are altered in *ret* mutant zebrafish hosts. (A) Amplitudes of periodic contraction along the intestine for wild-type (wt) and *ret* mutant zebrafish at 5 and 6 dpf. Shown are histograms with the percent of individual larvae within different amplitude ranges. Vertical dashed lines indicate median amplitudes for respective curves. $n = 28$ (5 dpf, wt); $n = 22$ (5 dpf, *ret*); $n = 29$ (6 dpf, wt); $n = 21$ (6 dpf, *ret*). (B) GF wild-type and *ret* heterozygous hosts (wt) were raised together with *ret* homozygous mutant hosts (*ret*) and colonized at 4 dpf with *Aeromonas*. At 5 (left) or 6 (right) dpf *Vibrio* was added to the water column for 24 hr prior to whole gut dissection and serial plating to enumerate bacterial abundances. Additionally plotted are respective *Aeromonas* mono-association reference (ref.) populations from Fig 1B (left, 4–6; right, 4–7). The difference between *Aeromonas* abundance during challenge and mono-association was determined by an unpaired *t* test. CFU = colony-forming units; *** = $p < 0.0001$; ns = not significant; $n > 18$/condition. Gray and black dashed lines denote limits of quantification and detection, respectively. Underlying data for A and B are provided in S1 Data.

doi:10.1371/journal.pbio.1002517.g006

specific model that connects contractile mechanics to transport of bacterial aggregates (i.e., the relationship between peristaltic amplitude and bacterial abundance), a quantitative mapping between these two observations is not possible. Transport of *Aeromonas*, for example, may depend non-linearly on contractile amplitude, or may depend on spatial or temporal features of complex intestinal motility patterns that are not captured by measurements of amplitude alone. Qualitatively, the difference in gut dynamics between wild-type and *ret* mutant hosts is clear (Fig 6A; S8 and S9 Movies), and our results ultimately provide evidence that ENS-driven intestinal motility contributes to the shaping of this model two-member community.

Discussion

Summary and Impact

A better understanding of the factors that influence the dynamics and stability of host-associated microbial communities would allow insights into their assembly [31–33], fluctuations during periods of normal health [12,14,15,34,35], and responses to perturbation [36,37], as well as aid the development of diagnostic and treatment strategies for human diseases [17]. Building a working knowledge of these processes has been impeded by the technical difficulties associated with examining bacterial populations within their native host environments. In humans, the approach generally taken has been to infer interspecies interactions from coarsely sampled sequencing-based metagenomic time-series experiments performed on fecal samples [12–14,35,38]. However, such procedures largely disregard spatial information and generally assume particular functional forms for interactions (e.g., deterministic Lotka-Volterra dynamics [12,14,15]). Moreover, measurement noise and missing information about absolute abundances in metagenomic data place severe limits on the quantitative determination of interaction strengths, even if the models are accurate descriptors of the microbial systems [12]. Therefore, basic questions regarding interspecies competition in the intestine, particularly the extent to which it is determined by the microbes themselves, properties of the gut environment, or a combination of the two, remain largely unanswered.

For these reasons, we set out to investigate bacterial population dynamics within the vertebrate intestine using a combination of absolute abundance measurements, time-series imaging, and quantitative modeling. Though our system is minimal, consisting of two bacterial species and a larval zebrafish host, it has revealed factors we expect to be of broad relevance to other animal-associated microbiota. Most notably, in this model system the competitive exclusion that is evident between *Aeromonas* and *Vibrio* is driven in large part by the physical activity of the host, namely the motility of the intestine. When introduced separately to zebrafish, each bacterial species is capable of robust intestinal colonization to high abundance, indicating an ability to make use of the resources present within the gut. When together, *Aeromonas* is largely excluded, as its enhanced sensitivity to physical disturbances renders it less capable of persisting within the gut environment. In mutant zebrafish that have reduced intestinal motility due to mutation of the gene *ret*, which impairs ENS development and function, competition between these bacterial species can be neutralized (Fig 6). Peristaltic motility and mass transport are, of course, key attributes of animal intestinal tracts. Importantly, the finding that the mechanical nature of the intestine has a major role in shaping bacterial communities suggests that models of microbiota based on in vitro competition assays or modeling of metabolic networks [16,39] will, by themselves, be insufficient for predicting and accurately describing community structure and dynamics. Consistent with this, a previous study has shown that dietary alteration of intestinal transit in a murine model led to compositional shifts in the gut microbiota [40].

Our study demonstrates a powerful mechanism by which host enteric neural activity can influence community composition. Interestingly, several recent investigations have

demonstrated the converse, that gut microbiota can alter intestinal motility through modulation of serotonin signaling [41], stimulation of macrophage-ENS crosstalk [42], and metabolism of bile salts [43]. These observations, together with the work presented here, suggest the possibility of an intricate feedback loop between the host and its microbiota based on intestinal motility. Corroborating this notion, human patients with Hirschsprung disease have been found to harbor dysbiotic microbial communities [44,45].

We were able to gain further insight into how intestinal motility contributes to stability and competition by constructing a quantitative model based on the observed *Aeromonas* dynamics, which consists of growth punctuated by stochastic collapses. Data derived from gut dissection, in which many fish are sampled at a single time point, can be fit to the model to determine its two relevant parameters, the bacterial carrying capacity, K, and a factor that characterizes the collapses, z. In itself, this is trivial. However, we can also determine z from independent, and quite different, data, namely image-based time-series of individual fish. The two measures agree, which provides strong support for the proposed stochastic-collapse-driven model of interspecies competition. Furthermore, the fit of the model to the data reveals that the impact of *Vibrio* on *Aeromonas* populations is twofold: reducing the overall carrying capacity and increasing sensitivity to physical perturbations, the combined effect of the two being much greater than that expected for either alone. More generally, our analysis provides evidence that quantitative, data-based models of interactions among species within the gut are possible, and that stochastic, rather than purely deterministic, dynamics can play a major role in shaping the composition and strength of competitive exclusion within intestinal communities. It is interesting to note that recent metagenomic analyses of human intestinal microbiota have uncovered signatures of sudden shifts in species composition, the origins of which remain unknown [15,46], perhaps indicating stochastic dynamics are widespread in natural intestinal systems.

From an ecological perspective, it is unsurprising that the physical environment and stochastic perturbations influence species abundance; these concepts are mainstays of our understanding of macroscopic multispecies communities [47]. A rich literature describes various stochastic population models and the characteristics, such as extinction probabilities, that emerge from them [48–51]. As shown here, it is likely that such models will in general be useful for providing a conceptual and predictive framework for understanding interspecies bacterial competition. Again mirroring well-established ecological concepts, we can frame our understanding of *Vibrio* and *Aeromonas* dynamics in the intestine as a study of these species' differential resistance and resilience to environmental perturbations. *Aeromonas* during mono-association is not resistant to disturbances related to intestinal motility, but it is resilient, able to grow to high abundances despite sporadic collapses. *Vibrio*, in contrast, is highly resistant to perturbations; it shows smooth growth unfazed by the environmental perturbations that affect *Aeromonas* (Fig 3). In the presence of *Vibrio*, both the resistance and resilience of *Aeromonas* are compromised, as the magnitude of collapses is greater and the carrying capacity to which to recover is diminished.

While ecological concepts can help us characterize microbial dynamics, data on microbial systems can, conversely, enhance our understanding of ecological theory. The fast generation time and high degree of reproducibility of microbial systems have allowed a variety of tests of ecological models in recent years, illuminating issues such as game-theoretic aspects of cheating [52], early warning indicators of population collapses [53], and the statistical structure of number fluctuations [54]. Although theoretical treatments of population collapses and extinction events are abundant in the ecological literature, real data with which to test them remain sparse [55], in part due to the challenges of performing high-precision field studies. We expect, therefore, that data of the sort presented here, which yield collapse statistics as well as fits to stochastic models, will have utility in contexts far removed from microbiota research.

The Relationship between Bacterial Traits and Population Stability

There is considerable medical interest in using specific bacterial strains (e.g., probiotics) or entire consortia (e.g., fecal microbiota transplants) to prevent or treat human disease. Central to these approaches will be to identify the fundamental traits of bacteria that influence population stability. We found that the differential susceptibility of our two model bacterial species to intestinal motility could be explained by their distinct community architectures. Highly motile single cells of *Vibrio* are relatively unaffected by intestinal contractions, which is in contrast to the large, non-motile aggregates of *Aeromonas* (Fig 4). Earlier observations of a related *A. veronii* strain showed higher growth rates for aggregated bacteria compared to planktonic bacteria [21], suggesting a tradeoff may exist in this lineage between enhanced growth and resistance to population-level disturbances. Curiously, in a murine microbiota model, antibodies able to recognize and bind to flagella were found to inhibit bacterial motility within the gut [56]. Together with our findings, this observation is provocative because it suggests that the host immune system and ENS might have the potential to work in tandem to tune the stability and persistence of a range of microbial lineages by acting on specific physiological traits. Food also has the potential to differentially interact with microbes within the confines of the intestinal environment. In preliminary work on conventionally raised larvae we find that, as expected, food increases the amplitude of intestinal motility, which might, all other things being equal, increase the likelihood of non-motile and aggregated bacteria like *Aeromonas* to be expelled. Alternatively, food that is broken down may supply additional surfaces for bacterial aggregation and growth, thereby lowering the chances of catastrophic population losses as lumenal contents are purged by peristalsis. Examining the consequences of feeding will likely reveal additional complexities of intestinal population dynamics. Going forward, we anticipate that to understand community dynamics within the intestine, the spatial structure and expression of bacterial traits, such as motility or aggregation, will be crucial.

Aeromonas population collapses are well described by stochastic dynamics, but the underlying mechanism by which *Vibrio* compromises resistance and resilience of *Aeromonas* remains to be elucidated. Several possibilities exist, and are the focus of ongoing investigation. *Vibrio* may disrupt the adhesive properties of sessile bacterial communities by secreting mucinases [57], or alter the rheological properties of the intestinal environment [58]. More directly, *Vibrio* may kill *Aeromonas* via secreted factors acting as bacteriocins or contact-mediated killing through the Type VI secretion system [59–61]. Intriguingly, it is unclear whether, in the context of a larger metacommunity composed of many fish in a shared aqueous environment, the aggregative tendencies of *Aeromonas* would actually put it at a competitive disadvantage compared to *Vibrio*. Expulsion of multicellular clusters could serve as a dispersal strategy by which new hosts are efficiently colonized by high-density founder populations of *Aeromonas*. This may explain the observation that species of *Vibrio* and *Aeromonas* are both highly represented among conventionally raised zebrafish [32]. If this is the case, then it implies that *Aeromonas* might have the capacity to respond to *Vibrio* invasion by altering its physiology and behavior to promote dispersal. The ways in which microbes interact and respond to each other in the complex intestinal milieu remains largely ill defined, but tractable gnotobiotic systems such as the one employed here will be instrumental in their exploration.

Outlook

The amenability of the larval zebrafish to gnotobiotic manipulation and imaging-based studies make it an ideal system for investigating host–microbe interactions across a range of complexities. For example, it will be possible to increase the diversity of interacting microbial species and examine emergent features of their competition, monitor the dynamics of immune

responses, observe and manipulate transmission between hosts, and introduce factors such as food or antibiotics to the intestinal environment. We expect that such studies will yield deeper insights into the dynamics of host-associated microbiota.

Methods

Ethics Statement

All experiments with zebrafish were done in accordance with protocols approved by the University of Oregon Institutional Animal Care and Use Committee and following standard protocols [62].

Gnotobiotic Techniques

Wild-type AB or *ret* mutant (*ret1*^{hu2846}, ZFIN ID: ZDB-ALT-070315-12) zebrafish were derived GF and colonized with bacterial strains as previously described [19]. Briefly, fertilized eggs from adult mating pairs were harvested and incubated in sterile embryo media (EM) containing 100 μg/ml ampicillin, 5 μg/ml kanamycin, and 250 μg/ml amphotericin B for ~6 hr. Embryos were then washed in EM containing 0.003% sodium hypochlorite followed by EM containing 0.1% polyvinylpyrrolidone–iodine. Sterilized embryos were distributed into T25 tissue culture flasks containing 15 ml sterile EM at a density of one embryo per ml and incubated at 28–30°C prior to bacterial colonization. Embryos were sustained on yolk-derived nutrients and not fed during experiments.

Bacterial Strains

Aeromonas (ZOR0001, PRJNA205571) and *Vibrio* (ZWU0020, PRJNA205585) were isolated from the zebrafish intestinal tract as described previously [24]. Fluorescently marked derivatives used in imaging experiments were engineered with an established Tn7 transposon-based approach [63]. Briefly, a cassette containing the constitutively active synthetic promoter Ptac cloned upstream of genes encoding dTomato or superfolder GFP was chromosomally inserted at the *attTn7* locus to generate *Aeromonas attTn7*::*Ptac-dTomato* and *Vibrio attTn7*::*Ptac-sfGFP*. Strains expressing fluorescent proteins did not exhibit overt fitness defects in vitro or in vivo. Prior to colonization at designated time points, bacterial strains were grown overnight in Luria Broth (LB) shaking at 30°C. Bacterial cultures were prepared for inoculation by pelleting for 2 min at 7,000 x g and washing once in sterile embryo medium (EM). An inoculum of 10^6 CFU/ml was used across experiments for each bacterial strain and added directly to the water column.

Culture-Based Quantification of Bacterial Populations

Dissection of larval guts was done as described previously [19]. Dissected guts were harvested and placed in a 1.6 ml tube containing 500 μl sterile 0.7% saline and ~100 μl 0.5 mm zirconium oxide beads (Next Advance, Averill Park, NY). Guts were then homogenized using a bullet blender tissue homogenizer (Next Advance, Averill Park, NY) for ~25 seconds on power 4. Lysates were serially plated on tryptic soy agar (TSA) and incubated overnight at 30°C prior to enumeration of CFU and determination of bacterial load. Plots depicting culture-based quantification of bacterial populations show the estimated limit of detection (5 bacteria/gut) as well as limit of quantification (100 bacteria/gut) and represent pooled data from a minimum of two independent experiments. Samples with zero countable colonies on the lowest dilution were set to the limit of detection prior to plotting and statistical analysis.

Light Sheet Microscopy

Imaging was performed using a home-built light sheet fluorescence microscope, based on the design of Keller et al. [18] and described in detail elsewhere [21,22]. Briefly, a laser beam is rapidly scanned with a galvanometer mirror and demagnified to provide a thin sheet of excitation light. An objective lens mounted perpendicular to the sheet captures fluorescence emission from the optical section, and the sample is scanned along the detection coordinate to yield a three-dimensional image. To image the entire extent of the intestine (approximately 1200x300x150 microns) we sequentially image four sub-regions and computationally register the images after acquisition. The entire volume of the intestine is imaged in less than 2 min in two colors, with a 1-micron spacing between planes. Unless otherwise indicated in the text, all exposure times are 30 ms with an excitation laser power of 5 mW, as measured between the theta-lens and the excitation objective.

Imaging-Based Quantification of Bacterial Populations

The analysis pipeline used to estimate bacterial abundances from light sheet imaging is described in [21]. In brief, we computationally identify both individual bacteria and clusters of bacteria, and estimate the population of each cluster by dividing the total fluorescence intensity by the average intensity of individual bacteria. As necessary, objects that are falsely identified as bacterial clusters are manually removed. For example, in Fig 3A an autofluorescent signal in the intestinal midgut in the *Vibrio* channel was excluded from subsequent quantitative analysis. Additionally, individual time points during time-series are removed if, determined by manual inspection, sample drift or motion of bacterial clusters driven by intestinal motility makes it infeasible to robustly estimate bacterial abundance.

Identification of Population Collapse Events

Collapses in bacteria populations are objectively identified from time-series of total bacterial abundance, such as those in Fig 3, by defining a collapse as a decrease in population by at least a factor of 10 within 1 hr. Collapse events with pre-collapse populations of less than 100 bacteria are discarded. These criteria were manually validated by associating each identified collapse with a corresponding ejection of bacteria from the gut observed in series of images.

Imaging Experiments

Sample mounting is done as previously described [21]. Larval zebrafish were removed from culture flasks and anaesthetized using 120 μg/ml tricaine methanesulfonate (Western Chemical, Ferndale, WA). Individual specimens were then briefly immersed in 0.5% agar (maximum temperature: 42°C) and drawn into a glass capillary, which was then mounted onto a sample holder. The agar-embedded specimens were partially extruded from the capillary so that the excitation and emission optical paths did not pass through glass interfaces. The specimen holder can hold up to six samples, all of which are immersed EM maintained at 28°C, with tricaine present as an anaesthetic. All long-term imaging experiments were done overnight, beginning in the late afternoon.

Measuring Bacterial Distance to Epithelial Wall

Individual bacteria were identified using the same algorithms used for quantification of bacterial abundance in the intestine. As we do not have a fluorescent marker for the epithelial wall of the intestine, we use the extent of the autofluorescent mucus in images as an estimate of the location of the epithelial wall. This extent is determined by active contour segmentation using

the Chan-Vese algorithm [64], using the implementation provided in MATLAB. A user-defined region is used as the seed for the segmentation of the first frame in the time-series, after which the segmentation of the previous frame is used as the seed for the segmentation of the subsequent frame. We then define the distance of each identified bacterium to the epithelial wall as the minimum distance between the location of the bacterium and the segmented extent of the intestine. Distributions of distances to the epithelial wall are constructed from all video frames and confidence intervals are obtained using bootstrap resampling. A null model of a uniform prediction is obtained by randomly distributing 1,000 points for each time point in the region defined by our intestinal segmentation. Confidence intervals are again obtained through bootstrap resampling.

Measuring Intestinal Motility

Larval intestinal motility was assessed from images captured using DIC microscopy, performed as previously described [28]. The displacement field from frame to frame in time-series was determined using particle image velocimetry (PIV) algorithms [65], which calculate the motions necessary for regions in one frame to be mapped onto regions in another. We focused our analysis on the frequency and amplitude of these motions, restricting our analysis to components of displacement along the intestinal axis. Fourier spectra of the displacements, averaged over location in the intestine, yielded in all cases a clear peak whose frequency and magnitude are indicative of the characteristic frequency and amplitude of intestinal motility, respectively. This method is described in greater detail in a forthcoming paper.

Supporting Information

S1 Data. Excel spreadsheet containing data values plotted in all main and supporting figures.
(XLSX)

S1 Fig. *Aeromonas* and *Vibrio* exhibit a competitive interaction within the larval zebrafish intestine. (A) Comparison of *Vibrio* abundances during mono-association and challenge of *Aeromonas* populations (see Fig 1A for succession scheme). (A, left) *Vibrio* abundances after different mono-association durations and (A, right) *Aeromonas* and *Vibrio* abundances after different *Vibrio* challenge periods. Statistical significance of *Vibrio* abundances after *Vibrio* challenge compared to respective mono-association reference populations (i.e., 5–6 versus 5–6; 6–7 versus 6–7; 5–7 versus 5–7) was determined by an unpaired *t* test. $^{*} = p < 0.05$; $^{***} = p < 0.0001$; ns = not significant; $n > 10$/condition. Founder populations "F" of (B) *Aeromonas* and (C) *Vibrio* were mono-associated with GF larvae on day 4 post-fertilization and challenged by fluorescently marked self populations "C" at 5 dpf for 24 hr (5–6) or 48 hr (5–7). Dissection and serial plating was done to enumerate founder and challenger populations. Counting of bacterial colonies was done on a fluorescent stereomicroscope. (D) Graphical overview of the reverse order succession schemes used in panel E. *Vibrio* was allowed to colonize GF larvae at 4 dpf followed by addition of *Aeromonas* to the water column at 5 dpf for 24 or 48 hr prior to enumeration of abundances by dissection and serial plating. (E, left) *Vibrio* and *Aeromonas* abundances after different mono-association durations. (E, right) *Aeromonas* and *Vibrio* abundances after different *Aeromonas* challenge periods. Statistical significance of abundances compared to respective mono-association reference populations (i.e., *Vibrio*: 4–6 versus 5–6, 4–7 versus 5–7; *Aeromonas*: 5–6 versus 5–6, 5–7 versus 5–7) was determined by an unpaired *t* test. $^{*} = p < 0.05$; $^{**} = p < 0.01$. (F) *Aeromonas* and *Vibrio* were inoculated into LB broth either individually or 1:1 and grown

overnight with shaking at 30°C prior to enumeration by serial plating. CFU = colony-forming units. Gray and black dashed lines in panels A, B, C, and F denote limit of quantification and detection, respectively. Underlying data for A–C, E, and F are provided in S1 Data.
(EPS)

S2 Fig. Space-filling properties of *Vibrio* within the zebrafish gut. (A) Single optical plane of 6 dpf larval zebrafish inoculated at 4 dpf with GFP-labeled *Vibrio*. Scale bar: 50 μm. (B–E) Blue curves: Spatial distribution of bacteria with respect to the approximate extent of the intestinal epithelial wall. Gray curves: prediction from a null model of uniform space filling. Each panel represents an individual fish with panel B being from the same specimen in panel A. Underlying data are provided in S1 Data.
(EPS)

S3 Fig. Collapses of *Aeromonas* populations within the zebrafish gut. (A) Total bacterial abundance derived from imaging data for *Aeromonas* and *Vibrio* for all imaged fish ($n = 13$) initially inoculated for 24 hr with *Aeromonas* and then challenged by *Vibrio*. Plots represent individual larvae and are plotted as a function of time following *Vibrio* inoculation. (B) Total bacterial abundance derived from imaging data for fish inoculated for 24 hr with *Aeromonas* alone ($n = 10$). Plots represent individual larvae and are plotted as a function of time following *Aeromonas* inoculation. (A and B) Vertical dashed lines indicate sharp drops of over an order of magnitude within an hour of the *Aeromonas* population. Underlying data for A and B are provided in S1 Data.
(EPS)

S4 Fig. Characteristics of zebrafish gut motility at 6 dpf for fish with different bacterial colonization histories. GF = germ-free; Aero = mono-association with *Aeromonas* from 4 dpf; Vibrio = mono-association with *Vibrio* from 4 dpf; Aer+Vib = mono-associated with *Aeromonas* at 4 dpf and challenged with *Vibrio* at 5 dpf. (A) The characteristic period of gut motility, identified as the inverse of the frequency of the peak signal in a Fourier spectrum of gut motion amplitudes, averaged over all positions. All conditions give very similar periodicity of gut motion. (B) The characteristic amplitude of gut motility, identified as magnitude of the peak signal in a Fourier spectrum of gut motion amplitudes. There is considerable variability between fish clutches, and so the amplitudes are normalized by the median of the germ-free fish in each batch. All conditions show large variance, with no significant difference evident between the various conditions. In A and B, gray X's are from individual fish; boxes indicate the first to third quartiles, and the horizontal bars in boxes indicates the median value. Underlying data for A and B are provided in S1 Data.
(TIF)

S5 Fig. Spatial distribution of *Aeromonas* and *Vibrio* during mono-association or challenge experiments. (A) Spatial distribution of *Vibrio*, quantified as the probability density along the gut, for 6 dpf fish mono-associated at 5 dpf with GFP-labeled *Vibrio* (gray) or inoculated at 4 dpf with dTomato-labeled *Aeromonas* and challenged at 5 dpf with GFP-labeled *Vibrio* (blue). (B) Probability density of *Aeromonas* in 6 dpf fish mono-associated at 5 dpf with dTomato-labeled *Aeromonas* (gray) or inoculated at 4 dpf with dTomato-labeled *Aeromonas* and challenged at 5 dpf with GFP-labeled *Vibrio* (magenta). The blue and magenta spatial distributions are drawn from the same fish. $n = 10$ for both conditions. Underlying data for A and B are provided in S1 Data.
(EPS)

S1 Movie. Example of the motile and planktonic behavior of *Vibrio* in the zebrafish gut. Live imaging of a single optical plane in the intestinal midgut of a 6 dpf larval zebrafish inoculated at 4 dpf with GFP-labeled *Vibrio*. Scale bar: 50 μm.
(AVI)

S2 Movie. Example of *Vibrio* space filling properties. Three-dimensional scan through the intestinal bulb of a 5 dpf larval zebrafish inoculated at 4 dpf with GFP-labeled *Vibrio*. Scale bar: 50 μm.
(AVI)

S3 Movie. Example of *Vibrio* resistance to intestinal contractions. Time-series is of a single optical plane in the intestinal bulb of a 6 dpf larval zebrafish inoculated at 4 dpf with GFP-labeled *Vibrio*. A subpopulation of *Vibrio* can be seen aggregating in the anterior bulb despite repeated intestinal contractions. Scale bar: 50 μm. Movie was recorded at 1 frame per second.
(AVI)

S4 Movie. Example of the non-motile and clustered behavior of *Aeromonas* in the zebrafish gut. Live imaging of a single optical plane in the intestinal midgut of a 6 dpf larval zebrafish inoculated at 4 dpf with dTomato-labeled *Aeromonas*. Scale bar: 50 μm.
(AVI)

S5 Movie. Spatial distribution of *Aeromonas* in the zebrafish gut. Three-dimensional scan through the intestinal bulb and midgut of a 5 dpf larval zebrafish inoculated at 4 dpf with dTomato-labeled *Aeromonas*. Bacterial clusters, individual bacteria (circled), and autofluorescent signals from intestinal mucus (gray haze) are indicated. Scale bar: 50 μm.
(AVI)

S6 Movie. Example of an *Aeromonas* collapse event during *Vibrio* challenge. Time-series is of maximum intensity projections of images taken from the same larval zebrafish shown in Fig 3A. The fish was initially colonized at 4 dpf with *Aeromonas* (magenta), challenged 24 hr later by inoculation with *Vibrio* (cyan), and then imaged every 20 min for 14 hr. Times indicate hours post-challenge. The region shown spans about 80% of the intestine, with the anterior on the left. Image contrast in both color channels is enhanced for clarity. Yellow dotted line roughly indicates the lumenal boundary of the intestine; the two bacterial fluorescence channels are overlaid inside this region. Scale bar: 200 μm.
(AVI)

S7 Movie. Example of *Aeromonas* sensitivity to intestinal contractions. Time-series is of a single optical plane in the intestinal midgut of a 6 dpf larval zebrafish inoculated at 4 dpf with dTomato-labeled *Aeromonas*. Scale bar: 50 μm. Movie was recorded at 1 frame per second.
(AVI)

S8 Movie. Example of intestinal motility in a wild-type larval zebrafish. DIC microscopy video of intestinal motility in a conventionally raised 6 dpf wild-type larval zebrafish. Scale bar: 50 μm.
(AVI)

S9 Movie. Example of intestinal motility in a *ret* mutant larval zebrafish. DIC microscopy video of intestinal motility in a conventionally raised 6 dpf *ret* mutant larval zebrafish. Scale bar: 50 μm.
(AVI)

S1 Program. MATLAB code used to simulate logistic growth punctuated by sudden drops in bacterial abundance.
(M)

S1 Text. PDF file containing description of stochastic collapse model.
(PDF)

Acknowledgments

We thank Michael Taormina (University of Oregon) for experimental advice and Brendan Bohannan (University of Oregon) and Pankaj Mehta (Boston University) for critical readings of the manuscript. For providing the zebrafish knockout allele *ret1-hu2846*, we thank the Hubrecht laboratory and the Sanger Institute Zebrafish Mutation Project.

Author Contributions

Conceived and designed the experiments: TJW MJ JSE KG RP. Performed the experiments: TJW MJ RPB JG. Analyzed the data: TJW MJ RPB BHS SLL RP. Contributed reagents/materials/analysis tools: TJW MJ RPB EM. Wrote the paper: TJW MJ JSE KG RP.

References

1. Cox LM, Yamanishi S, Sohn J, Alekseyenko AV, Leung JM, Cho I, et al. Altering the intestinal microbiota during a critical developmental window has lasting metabolic consequences. Cell. 2014; 158 (4):705–21. doi: 10.1016/j.cell.2014.05.052 PMID: 25126780; PubMed Central PMCID: PMC4134513.
2. Semova I, Carten JD, Stombaugh J, Mackey LC, Knight R, Farber SA, et al. Microbiota regulate intestinal absorption and metabolism of fatty acids in the zebrafish. Cell Host Microbe. 2012; 12(3):277–88. doi: 10.1016/j.chom.2012.08.003 PMID: 22980325; PubMed Central PMCID: PMC3517662.
3. Round JL, Mazmanian SK. The gut microbiota shapes intestinal immune responses during health and disease. Nat Rev Immunol. 2009; 9(5):313–23. doi: 10.1038/nri2515 PMID: 19343057; PubMed Central PMCID: PMC4095778.
4. Goyal MS, Venkatesh S, Milbrandt J, Gordon JI, Raichle ME. Feeding the brain and nurturing the mind: Linking nutrition and the gut microbiota to brain development. Proc Natl Acad Sci U S A. 2015; 112 (46):14105–12. doi: 10.1073/pnas.1511465112 PMID: 26578751; PubMed Central PMCID: PMC4655552.
5. McKenney PT, Pamer EG. From Hype to Hope: The Gut Microbiota in Enteric Infectious Disease. Cell. 2015; 163(6):1326–32. doi: 10.1016/j.cell.2015.11.032 PMID: 26638069; PubMed Central PMCID: PMC4672394.
6. Nicholson JK, Holmes E, Kinross J, Burcelin R, Gibson G, Jia W, et al. Host-gut microbiota metabolic interactions. Science. 2012; 336(6086):1262–7. doi: 10.1126/science.1223813 PMID: 22674330.
7. Lawley TD, Walker AW. Intestinal colonization resistance. Immunology. 2013; 138(1):1–11. doi: 10.1111/j.1365-2567.2012.03616.x PMID: 23240815; PubMed Central PMCID: PMC3533696.
8. Rainey PB, Travisano M. Adaptive radiation in a heterogeneous environment. Nature. 1998; 394 (6688):69–72. doi: 10.1038/27900 PMID: 9665128.
9. Kim HJ, Boedicker JQ, Choi JW, Ismagilov RF. Defined spatial structure stabilizes a synthetic multispecies bacterial community. Proc Natl Acad Sci U S A. 2008; 105(47):18188–93. doi: 10.1073/pnas.0807935105 PMID: 19011107; PubMed Central PMCID: PMC2587551.
10. Hol FJ, Galajda P, Nagy K, Woolthuis RG, Dekker C, Keymer JE. Spatial structure facilitates cooperation in a social dilemma: empirical evidence from a bacterial community. PLoS ONE. 2013; 8(10): e77042. doi: 10.1371/journal.pone.0077042 PMID: 24167557; PubMed Central PMCID: PMC3805552.
11. Coyte KZ, Schluter J, Foster KR. The ecology of the microbiome: Networks, competition, and stability. Science. 2015; 350(6261):663–6. doi: 10.1126/science.aad2602 PMID: 26542567.
12. Fisher CK, Mehta P. Identifying keystone species in the human gut microbiome from metagenomic timeseries using sparse linear regression. PLoS ONE. 2014; 9(7):e102451. doi: 10.1371/journal.pone.0102451 PMID: 25054627; PubMed Central PMCID: PMC4108331.

13. Friedman J, Alm EJ. Inferring correlation networks from genomic survey data. PLoS Comput Biol. 2012; 8(9):e1002687. doi: 10.1371/journal.pcbi.1002687 PMID: 23028285; PubMed Central PMCID: PMC3447976.
14. Stein RR, Bucci V, Toussaint NC, Buffie CG, Ratsch G, Pamer EG, et al. Ecological modeling from time-series inference: insight into dynamics and stability of intestinal microbiota. PLoS Comput Biol. 2013; 9(12):e1003388. doi: 10.1371/journal.pcbi.1003388 PMID: 24348232; PubMed Central PMCID: PMC3861043.
15. Trosvik P, de Muinck EJ, Stenseth NC. Biotic interactions and temporal dynamics of the human gastrointestinal microbiota. ISME J. 2015; 9(3):533–41. doi: 10.1038/ismej.2014.147 PMID: 25148482; PubMed Central PMCID: PMC4331571.
16. Levy R, Borenstein E. Metabolic modeling of species interaction in the human microbiome elucidates community-level assembly rules. Proc Natl Acad Sci U S A. 2013; 110(31):12804–9. doi: 10.1073/pnas.1300926110 PMID: 23858463; PubMed Central PMCID: PMC3732988.
17. Fischbach MA, Segre JA. Signaling in Host-Associated Microbial Communities. Cell. 2016; 164 (6):1288–300. doi: 10.1016/j.cell.2016.02.037 PMID: 26967294.
18. Keller PJ, Schmidt AD, Wittbrodt J, Stelzer EH. Reconstruction of zebrafish early embryonic development by scanned light sheet microscopy. Science. 2008; 322(5904):1065–9. doi: 10.1126/science.1162493 PMID: 18845710.
19. Milligan-Myhre K, Charette JR, Phennicie RT, Stephens WZ, Rawls JF, Guillemin K, et al. Study of host-microbe interactions in zebrafish. Methods Cell Biol. 2011; 105:87–116. doi: 10.1016/B978-0-12-381320-6.00004–7 PMID: 21951527.
20. Dooley K, Zon LI. Zebrafish: a model system for the study of human disease. Curr Opin Genet Dev. 2000; 10(3):252–6. PMID: 10826982.
21. Jemielita M, Taormina MJ, Burns AR, Hampton JS, Rolig AS, Guillemin K, et al. Spatial and temporal features of the growth of a bacterial species colonizing the zebrafish gut. MBio. 2014; 5(6). doi: 10.1128/mBio.01751-14 PMID: 25516613; PubMed Central PMCID: PMC4271548.
22. Taormina MJ, Jemielita M, Stephens WZ, Burns AR, Troll JV, Parthasarathy R, et al. Investigating bacterial-animal symbioses with light sheet microscopy. Biol Bull. 2012; 223(1):7–20. PMID: 22983029; PubMed Central PMCID: PMC3952068.
23. Roeselers G, Mittge EK, Stephens WZ, Parichy DM, Cavanaugh CM, Guillemin K, et al. Evidence for a core gut microbiota in the zebrafish. ISME J. 2011; 5(10):1595–608. doi: 10.1038/ismej.2011.38 PMID: 21472014; PubMed Central PMCID: PMC3176511.
24. Stephens WZ, Burns AR, Stagaman K, Wong S, Rawls JF, Guillemin K, et al. The composition of the zebrafish intestinal microbial community varies across development. ISME J. 2015. doi: 10.1038/ismej.2015.140 PMID: 26339860.
25. Rolig AS, Parthasarathy R, Burns AR, Bohannan BJ, Guillemin K. Individual Members of the Microbiota Disproportionately Modulate Host Innate Immune Responses. Cell Host Microbe. 2015; 18(5):613–20. doi: 10.1016/j.chom.2015.10.009 PMID: 26567512.
26. Drescher K, Dunkel J, Cisneros LH, Ganguly S, Goldstein RE. Fluid dynamics and noise in bacterial cell-cell and cell-surface scattering. Proc Natl Acad Sci U S A. 2011; 108(27):10940–5. doi: 10.1073/pnas.1019079108 PMID: 21690349; PubMed Central PMCID: PMC3131322.
27. Cocchiaro JL, Rawls JF. Microgavage of zebrafish larvae. J Vis Exp. 2013;(72:):e4434. doi: 10.3791/4434 PMID: 23463135; PubMed Central PMCID: PMC3605733.
28. Baker RP, Taormina MJ, Jemielita M, Parthasarathy R. A combined light sheet fluorescence and differential interference contrast microscope for live imaging of multicellular specimens. J Microsc. 2015; 258(2):105–12. doi: 10.1111/jmi.12220 PMID: 25611324; PubMed Central PMCID: PMC4401621.
29. Hanson FB, Tuckwell HC. Logistic growth with random density independent disasters. Theoretical Population Biology. 1981; 19(1):Pages 1–18.
30. Heanue TA, Pachnis V. Ret isoform function and marker gene expression in the enteric nervous system is conserved across diverse vertebrate species. Mech Dev. 2008; 125(8):687–99. doi: 10.1016/j.mod.2008.04.006 PMID: 18565740.
31. Sonnenburg JL, Angenent LT, Gordon JI. Getting a grip on things: how do communities of bacterial symbionts become established in our intestine? Nat Immunol. 2004; 5(6):569–73. doi: 10.1038/ni1079 PMID: 15164016.
32. Burns AR, Stephens WZ, Stagaman K, Wong S, Rawls JF, Guillemin K, et al. Contribution of neutral processes to the assembly of gut microbial communities in the zebrafish over host development. ISME J. 2015. doi: 10.1038/ismej.2015.142 PMID: 26296066.

33. Shafquat A, Joice R, Simmons SL, Huttenhower C. Functional and phylogenetic assembly of microbial communities in the human microbiome. Trends Microbiol. 2014; 22(5):261–6. doi: 10.1016/j.tim.2014.01.011 PMID: 24618403; PubMed Central PMCID: PMC4008634.

34. Rajilic-Stojanovic M, Heilig HG, Tims S, Zoetendal EG, de Vos WM. Long-term monitoring of the human intestinal microbiota composition. Environ Microbiol. 2012. doi: 10.1111/1462-2920.12023 PMID: 23286720.

35. Caporaso JG, Lauber CL, Costello EK, Berg-Lyons D, Gonzalez A, Stombaugh J, et al. Moving pictures of the human microbiome. Genome Biol. 2011; 12(5):R50. doi: 10.1186/gb-2011-12-5-r50 PMID: 21624126; PubMed Central PMCID: PMC3271711.

36. Allison SD, Martiny JB. Colloquium paper: resistance, resilience, and redundancy in microbial communities. Proc Natl Acad Sci U S A. 2008; 105 Suppl 1:11512–9. doi: 10.1073/pnas.0801925105 PMID: 18695234; PubMed Central PMCID: PMC2556421.

37. Dethlefsen L, Relman DA. Incomplete recovery and individualized responses of the human distal gut microbiota to repeated antibiotic perturbation. Proc Natl Acad Sci U S A. 2011; 108 Suppl 1:4554–61. doi: 10.1073/pnas.1000087107 PMID: 20847294; PubMed Central PMCID: PMC3063582.

38. Faust K, Raes J. Microbial interactions: from networks to models. Nat Rev Microbiol. 2012; 10(8):538–50. doi: 10.1038/nrmicro2832 PMID: 22796884.

39. Klitgord N, Segre D. Environments that induce synthetic microbial ecosystems. PLoS Comput Biol. 2010; 6(11):e1001002. doi: 10.1371/journal.pcbi.1001002 PMID: 21124952; PubMed Central PMCID: PMC2987903.

40. Kashyap PC, Marcobal A, Ursell LK, Larauche M, Duboc H, Earle KA, et al. Complex interactions among diet, gastrointestinal transit, and gut microbiota in humanized mice. Gastroenterology. 2013; 144(5):967–77. doi: 10.1053/j.gastro.2013.01.047 PMID: 23380084; PubMed Central PMCID: PMC3890323.

41. Yano JM, Yu K, Donaldson GP, Shastri GG, Ann P, Ma L, et al. Indigenous bacteria from the gut microbiota regulate host serotonin biosynthesis. Cell. 2015; 161(2):264–76. doi: 10.1016/j.cell.2015.02.047 PMID: 25860609; PubMed Central PMCID: PMC4393509.

42. Muller PA, Koscso B, Rajani GM, Stevanovic K, Berres ML, Hashimoto D, et al. Crosstalk between muscularis macrophages and enteric neurons regulates gastrointestinal motility. Cell. 2014; 158(2):300–13. doi: 10.1016/j.cell.2014.04.050 PMID: 25036630; PubMed Central PMCID: PMC4149228.

43. Dey N, Wagner VE, Blanton LV, Cheng J, Fontana L, Haque R, et al. Regulators of gut motility revealed by a gnotobiotic model of diet-microbiome interactions related to travel. Cell. 2015; 163(1):95–107. doi: 10.1016/j.cell.2015.08.059 PMID: 26406373; PubMed Central PMCID: PMC4583712.

44. Frykman PK, Nordenskjold A, Kawaguchi A, Hui TT, Granstrom AL, Cheng Z, et al. Characterization of Bacterial and Fungal Microbiome in Children with Hirschsprung Disease with and without a History of Enterocolitis: A Multicenter Study. PLoS ONE. 2015; 10(4):e0124172. doi: 10.1371/journal.pone.0124172 PMID: 25909773; PubMed Central PMCID: PMC4409062.

45. Gosain A, Brinkman AS. Hirschsprung's associated enterocolitis. Curr Opin Pediatr. 2015; 27(3):364–9. doi: 10.1097/MOP.0000000000000210 PMID: 25944307; PubMed Central PMCID: PMC4451822.

46. David LA, Materna AC, Friedman J, Campos-Baptista MI, Blackburn MC, Perrotta A, et al. Host lifestyle affects human microbiota on daily timescales. Genome Biol. 2014; 15(7):R89. doi: 10.1186/gb-2014-15-7-r89 PMID: 25146375; PubMed Central PMCID: PMC4405912.

47. Sousa WP. The Role of Disturbance in Natural Communities. Annual Review of Ecology and Systematics. 1984; 15: 353–91. doi: 10.1146/annurev.es.15.110184.002033

48. Ovaskainen O, Meerson B. Stochastic models of population extinction. Trends Ecol Evol. 2010; 25(11):643–52. doi: 10.1016/j.tree.2010.07.009 PMID: 20810188.

49. Melbourne BA, Hastings A. Extinction risk depends strongly on factors contributing to stochasticity. Nature. 2008; 454(7200):100–3. doi: 10.1038/nature06922 PMID: 18596809.

50. Allen LJ, Allen EJ. A comparison of three different stochastic population models with regard to persistence time. Theor Popul Biol. 2003; 64(4):439–49. PMID: 14630481.

51. Lande R. Risks of Population Extinction from Demographic and Environmental Stochasticity and Random Catastrophes. The American Naturalist. 1993; 142(6):911–27.

52. Gore J, Youk H, van Oudenaarden A. Snowdrift game dynamics and facultative cheating in yeast. Nature. 2009; 459(7244):253–6. doi: 10.1038/nature07921 PMID: 19349960; PubMed Central PMCID: PMC2888597.

53. Dai L, Vorselen D, Korolev KS, Gore J. Generic indicators for loss of resilience before a tipping point leading to population collapse. Science. 2012; 336(6085):1175–7. doi: 10.1126/science.1219805 PMID: 22654061.

54. Frentz Z, Kuehn S, Leibler S. Strongly Deterministic Population Dynamics in Closed Microbial Communities. Physical Review X. 2015; 5(4):041014.

55. Carpenter SR, Cole JJ, Pace ML, Batt R, Brock WA, Cline T, et al. Early warnings of regime shifts: a whole-ecosystem experiment. Science. 2011; 332(6033):1079–82. doi: 10.1126/science.1203672 PMID: 21527677.

56. Cullender TC, Chassaing B, Janzon A, Kumar K, Muller CE, Werner JJ, et al. Innate and adaptive immunity interact to quench microbiome flagellar motility in the gut. Cell Host Microbe. 2013; 14 (5):571–81. doi: 10.1016/j.chom.2013.10.009 PMID: 24237702; PubMed Central PMCID: PMC3920589.

57. Szabady RL, Yanta JH, Halladin DK, Schofield MJ, Welch RA. TagA is a secreted protease of Vibrio cholerae that specifically cleaves mucin glycoproteins. Microbiology. 2011; 157(Pt 2):516–25. doi: 10.1099/mic.0.044529–0 PMID: 20966091; PubMed Central PMCID: PMC3090133.

58. Celli JP, Turner BS, Afdhal NH, Keates S, Ghiran I, Kelly CP, et al. Helicobacter pylori moves through mucus by reducing mucin viscoelasticity. Proc Natl Acad Sci U S A. 2009; 106(34):14321–6. doi: 10.1073/pnas.0903438106 PMID: 19706518; PubMed Central PMCID: PMC2732822.

59. Wexler AG, Bao Y, Whitney JC, Bobay LM, Xavier JB, Schofield WB, et al. Human symbionts inject and neutralize antibacterial toxins to persist in the gut. Proc Natl Acad Sci U S A. 2016. doi: 10.1073/pnas.1525637113 PMID: 26957597.

60. Basler M, Mekalanos JJ. Type 6 secretion dynamics within and between bacterial cells. Science. 2012; 337(6096):815. doi: 10.1126/science.1222901 PMID: 22767897; PubMed Central PMCID: PMC3557511.

61. Basler M, Ho BT, Mekalanos JJ. Tit-for-tat: type VI secretion system counterattack during bacterial cell-cell interactions. Cell. 2013; 152(4):884–94. doi: 10.1016/j.cell.2013.01.042 PMID: 23415234; PubMed Central PMCID: PMC3616380.

62. Westerfield M. The zebrafish book. A guide for the laboratory use of zebrafish (Danio rerio). 4th ed: University of Oregon Press, Eugene; 2000.

63. Choi KH, Gaynor JB, White KG, Lopez C, Bosio CM, Karkhoff-Schweizer RR, et al. A Tn7-based broad-range bacterial cloning and expression system. Nat Methods. 2005; 2(6):443–8. doi: 10.1038/nmeth765 PMID: 15908923.

64. Chan TFV, L.A. Active Contours Without Edges. IEEE Transactions on Image Processing. 2001; 10 (2):266–77. doi: 10.1109/83.902291 PMID: 18249617

65. Thielicke WS E.J. PIVlab–Towards User-friendly, Affordable and Accurate Digital Particle Image Velocimetry in MATLAB. Journal of Open Research Software. 2014; 2(1). http://doi.org/10.5334/jors.bl.